

## Synthesis of calcium polysulfides at high pressures

Sheng Wang,<sup>1,\*</sup> Wencheng Lu,<sup>1,\*</sup> Siyu Liu,<sup>1</sup> Mi Zhou,<sup>1</sup> Pengyue Gao,<sup>1,†</sup> Hongbo Wang,<sup>1</sup> Jian Lv,<sup>1</sup> Huiyang Gou,<sup>2</sup> Guangtao Liu<sup>1,‡</sup>, Hanyu Liu,<sup>1,3</sup> Yanchao Wang<sup>1</sup> and Yanming Ma<sup>1,3</sup>

<sup>1</sup>State Key Laboratory of Superhard Materials and International Center of Computational Method & Software, College of Physics, Jilin University, Changchun 130012, China

<sup>2</sup>Center for High Pressure Science and Technology Advanced Research, Beijing 100094, China

<sup>3</sup>International Center of Future Science, Jilin University, Changchun 130012, China

HPSTAR  
1237-2021



(Received 2 June 2021; revised 20 July 2021; accepted 3 August 2021; published 25 August 2021)

Chalcogenides have attracted wide attention on the structural characterizations and physicochemical properties due to their potential practicability and scientific interests, such as the intriguing stoichiometries and involved fascinating morphologies of sulfur under compression. In this work, our *ab initio* structure prediction simulations for the Ca-S system predicted unprecedented tetragonal  $I4/mcm$ -CaS<sub>2</sub> and  $P-42_1m$ -CaS<sub>3</sub> containing the isolated dimeric S<sub>2</sub><sup>2-</sup> and V-shape trimeric S<sub>3</sub><sup>2-</sup> units, respectively, under high pressure. Motivated by these theoretical results, remarkably, we have successfully synthesized CaS<sub>2</sub> and CaS<sub>3</sub> as unambiguously identified through *in situ* x-ray diffraction and Raman spectra measurements. The present results have unraveled the high-pressure structure behavior of Ca-S system and further provided key insights for exploring other interesting polysulfides at extreme conditions.

DOI: [10.1103/PhysRevB.104.054117](https://doi.org/10.1103/PhysRevB.104.054117)

### I. INTRODUCTION

In recent decades, alkaline-earth metal sulfides (AESs, AE = Be, Mg, Ca, Sr, Ba) have attracted considerable interest and were extensively investigated in experimental and theoretical studies, due to their excellent technical applicability as large band-gap semiconductors applied in microelectronic and luminescent devices, etc. [1–3]. Normally, these compounds crystallize in a NaCl-type structure with  $Fm-3m$  symmetry (except for BeS) at ambient conditions, that essentially determines their basic physicochemical properties. Moreover, these AES compounds undergo a representative structural phase transition from the ambient NaCl-type ( $Fm-3m$ ) structure to a CsCl-type one ( $Pm-3m$ ) under compression, accompanying with atomic reconstructions [4]. Actually, pressure plays an indispensable role in altering the interatomic distances and bonding patterns, which can result in phase transitions and the appearances of unprecedented compounds with intriguing stoichiometries [5–10]. These newfangled high-pressure compounds not only possess outstanding performance unavailable at ambient conditions (such as compelling high-temperature superconductivities in polyhydrides [11–13]), but also bring new perceptions of Earth's evolution (such as unique FeO<sub>2</sub> providing an interpretation of oxygen circulation in earth [14]).

A series of experimental and theoretical investigations have explored the AES<sub>x</sub> family and extended the number of alkaline-earth polysulfides under pressure. In past decades,

unconventional BaS<sub>2</sub>, BaS<sub>3</sub>, Ba<sub>2</sub>S<sub>3</sub>, SrS<sub>2</sub>, and SrS<sub>3</sub> were synthesized under high pressures [15–18]. Recently, a theoretical work suggested that BeS<sub>2</sub> with  $Pa-3$  symmetry can be stable from 25 GPa to at least 100 GPa as a direct band-gap semiconductor, which may have potential applications in optical and electrical technologies [19]. Although calcium is one of the most abundant elements on earth and forms lots of significant compounds, there has been no information on calcium polysulfide until very recently. In 2021, moreover, Liu *et al.* theoretically investigated the stability of the Ca-S system above 50 GPa and proposed that the metallic CaS<sub>x</sub> compounds are superconductors [20]. Therefore, it is still an open question to further investigate, especially for experiment, the details of various CaS<sub>x</sub> compounds under compression, motivated by the following objectives: (i) to study the stability of traditional CaS in considering any possible decomposition; (ii) to explore whether the new CaS<sub>x</sub> compounds can be synthesized at moderate conditions; (iii) to determine the ground-state structures and relative properties of CaS<sub>x</sub> under high pressure; and (iv) even to regulate the involved valence states of sulfur or its unit.

Here, we conducted a joint theoretical and experimental exploration on the compressed Ca-S system. We performed a theoretical structure prediction for the Ca-S compounds under pressures below 50 GPa using the state-of-the-art swarm intelligence algorithm combined with the *ab initio* simulation, and carried out the following high-temperature-pressure experimental work. Here, we propose a high-pressure  $I4/mcm$  CaS<sub>2</sub> phase with S<sub>2</sub><sup>2-</sup> units and have synthesized the CaS<sub>2</sub> and CaS<sub>3</sub> structures with precursors of Ca and S at about 21 GPa/2500 K and 34 GPa/2500 K, respectively. Both x-ray diffraction (XRD) and Raman spectra experiments confirmed that their crystal structures are in very good

\*These authors contributed equally to this work.

†Corresponding author: gpy@calypso.cn

‡Corresponding author: liuguangtao@jlu.edu.cn

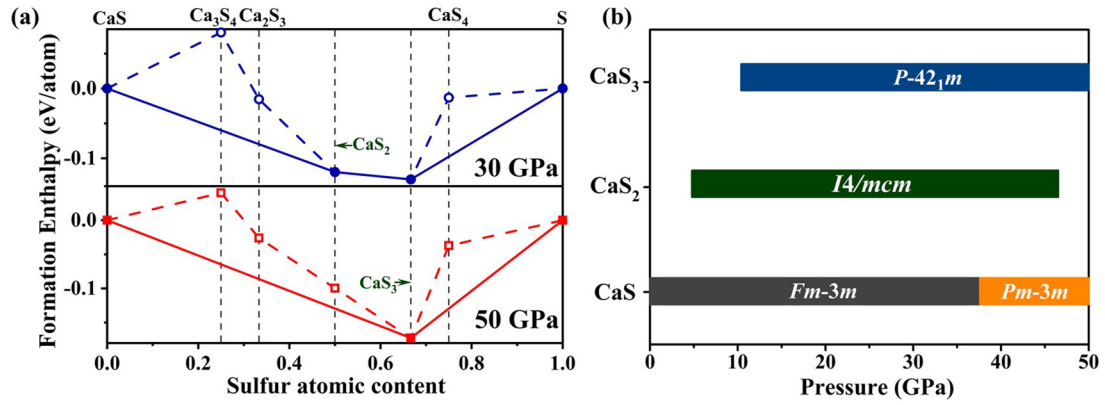


FIG. 1. (a) Ground-state and static enthalpies of formation per atom of the  $\text{CaS}_x$  phases at 30 and 50 GPa. The symbols on the solid lines denote that the sulfides are stable at the corresponding pressure, while those on the dashed lines represent that the sulfides are unstable with respect to their decomposition into elements or other sulfides. (b) Stable phases and their range of pressure of the Ca-S system.

agreement with our theoretical proposals, that provides reliable insights for the understanding of the compressed Ca-S system.

## II. METHODS

### A. Calculations

The crystal structure predictions of CaS, CaS<sub>2</sub>, CaS<sub>3</sub>, CaS<sub>4</sub>, Ca<sub>2</sub>S<sub>3</sub>, and Ca<sub>3</sub>S<sub>4</sub> within 40 atoms were based on the state-of-the-art particle swarm optimization technique implemented in our developed CALYPSO code [21–23] at 0, 10, 30, and 50 GPa, which has been developed for years as a powerful method for predicting unprecedented materials with given pressures and chemical positions [6–9], and solving structural conundrums in experiments [24,25]. All structural relaxations and most of the property simulations were performed using the projector augmented-wave (PAW) [26] method with Perdew-Burke-Ernzerhof (PBE) exchange correlation function [27] in the *Vienna ab initio simulation* (VASP) code [28]. Raman simulations were performed with the local density approximation (LDA) and generalized gradient approximation (GGA) functions [29]. The  $3p^6 4s^2$  and  $3s^2 3p^2$  serve as the valence electrons for Ca and S, respectively. The kinetic cutoff energy of electronic wave functions was set to 600 eV and appropriate Monkhorst-Pack  $k$  meshes were used to ensure that the enthalpy calculations are converged to better than 1 meV/atom in all cases. Phonon calculations were carried out using the PHONOPY code [30,31] to check the dynamical stabilities of the candidate structures.

### B. Experiments

In experimental study, samples were prepared in a glove-box with Ar atmosphere that had low contents of O<sub>2</sub> and H<sub>2</sub>O (less than 0.01 ppm). Elemental calcium and sulfur powder were compressed into flakes with thickness of  $\sim 2$   $\mu\text{m}$  and loaded into a sample chamber (100  $\mu\text{m}$ ) with a preindented T301 steel gasket. CaF<sub>2</sub> was used and formed a sandwichlike structure as both a thermal insulator layer and pressure media sticking to the culets with diameter of 300  $\mu\text{m}$ . Pressures were determined by diamond Raman edge [32]. Compressed

samples were heated with an off-line pulsed infrared laser and temperatures were estimated by fitting the thermal radiation spectra to the Planck radiation function. Room-temperature Raman spectra were excited by a 633-nm laser and recorded by a homemade spectrometer (SpectraPro HRS-500 equipped with a PyLoN:100 charge-coupled device, Princeton Instruments). The typical exposure time of Raman is about 10 sec. *In situ* high-pressure angle-dispersive synchrotron XRD data were collected to investigated crystal structures at room temperature at BL15U1 of the Shanghai Synchrotron Radiation Facility and BL4W2 of the Beijing Synchrotron Radiation Facility ( $\lambda = 0.6199$   $\text{\AA}$ ). For XRD measurements, the x-ray beam sizes and exposure time are about  $3 \times 5$  and  $10 \times 30$   $\mu\text{m}^2$ , and 30 and 600 sec for BL15U1 and BL4W2, respectively. The sample-detector distance and other geometric parameters were calibrated using a CeO<sub>2</sub> standard. Two-dimension Bragg diffraction patterns were collected using a MAR-345 image plate detector and analyzed using FIT2D software [33], integrating powder diffraction rings and converting the two-dimensional data to one-dimensional profiles. Rietveld profile matching refinements were performed using the GSAS + EXPGUI programs [34,35].

## III. RESULTS AND DISCUSSION

### A. Stability of CaS<sub>x</sub> under high pressures

First, the known ambient structure (*Fm-3m*) of CaS and its high-pressure phase (*Pm-3m*) as well as the experimental phase transition pressure ( $37.1 \pm 2.9$  GPa) were successfully reproduced in this work, confirming the reliability of our structure prediction method and simulations that make our following work more convincing. These two phases and sulfur [36,37] corresponding to the applied pressures are adopted to investigate the stabilities of other stoichiometric calcium polysulfides. Therefore, their formation enthalpies relative to CaS and sulfur substance are defined as

$$\Delta H_f(\text{Ca}_x\text{S}_y) = [H(\text{Ca}_x\text{S}_y) - xH(\text{CaS}) - (y-x)H(\text{S})]/(x+y)$$

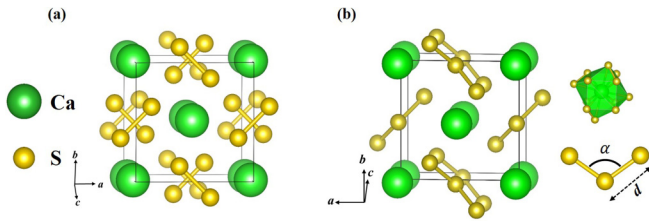


FIG. 2. The crystal structures of (a)  $\text{CaS}_2$  ( $I4/mcm$ ) and (b)  $\text{CaS}_3$  ( $P-42_1m$ ) at 30 GPa. Large green and small yellow spheres represent Ca and S atoms, respectively.

and calculated convex hulls [Fig. 1(a)] were plotted to describe the considered structures, where the stoichiometries lying on the solid lines are thermodynamic stable under the corresponding pressure. By contrast, others on the dashed lines will decompose into the adjacent compounds or elements from the perspective of energy. As shown in Fig. 1(a), the predicted  $\text{CaS}_3$  and  $\text{CaS}_2$  become thermodynamically stable at elevated pressures. In order to estimate their detailed formation and decomposition pressures, we further calculated and plotted the pressure-composition phase diagram [Fig. 1(b)]. Conventional  $\text{CaS}$  always exists with respect to elements or other compounds during the whole range of pressure in this study;  $\text{CaS}_3$  is calculated to be stable above  $\sim 10$  GPa; and  $\text{CaS}_2$  is energetically preferable between  $\sim 5$  and 45 GPa, then tends to decompose into the adjacent  $\text{CaS}$  and  $\text{CaS}_3$  compounds. In addition to the thermal stability, the phonon band structures were also calculated to guarantee the dynamical stabilities of the predicted compounds. It is clear that no imaginary phonon mode exists at the given pressures (see the Supplemental Material (SM)) [38], which confirms the stabilities of these two structures.

The predicted  $\text{CaS}_2$  structure is isomorphic with other alkaline-earth metal chalcogenides such as  $\text{CaO}_2$ ,  $\text{SrS}_2$ , and  $\text{BaTe}_2$  [Fig. 2(a)] [17,39,40]. It contains the dimeric sul-

fur units ( $\text{S}_2^{2-}$ ) which lie in layers perpendicular to the (001) direction and the units are arranged oppositely to the counterparts in adjacent layer. Ca atoms lying between the layers are surrounded by eight sulfur atoms. The S-S bond length is calculated to be 2.08 Å at 10 GPa and decreases slightly to 2.02 Å at 30 GPa.  $\text{CaS}_3$  containing the isolated V-shaped trimeric sulfur ( $\text{S}_3$ ) unit crystallizes in a  $\text{BaS}_3$ -type structure [15]. Viewed along the  $c$  axis, the  $\text{S}_3^{2-}$  units are located at the face centers around the  $c$  axis. Ca atoms occupying the body center or edge centers are surrounded by 12 sulfur atoms. The theoretical S-S bond length and S-S-S bond angle of the  $\text{S}_3^{2-}$  unit are 2.05 Å, 108.9° at 30 GPa and reduced to 2.03 Å, 105.9° with the pressure increasing to 50 GPa. We also note the same proposal of  $\text{CaS}_3$  structure [Fig. 2(b)] in the recent report [20], that shares the similar configuration in  $\text{BaS}_3$ ,  $\text{SrS}_3$ , and  $\text{CaO}_3$  [15,18,41].

Since the stability of the system may be influenced at the finite temperature, the entropy of vibration of each structure is considered and the phase boundaries were estimated by Gibbs free energy based on the quasiharmonic approximation, as shown in the SM [38].  $\text{CaS}_2$  and  $\text{CaS}_3$  are still stable at higher temperature, but the stable range of  $\text{CaS}_2$  becomes a little bit narrow compared to that at zero temperature.

## B. Syntheses and vibrational properties

Inspired by the above systematic enthalpy simulations on calcium polysulfides, we further performed related experiments employing laser-heated diamond anvil cell (DAC) to check whether anticipated  $\text{CaS}_2$  and  $\text{CaS}_3$  can be synthesized at appropriate conditions. Before laser heating, only Raman signals of amorphous or III-phase S can be observed in the compressed mixed precursors (Fig. 3) ( $\text{CaS}$  has no Raman mode), indicating that high temperature is necessary to overcome the barrier of expected chemical reactions.

Then, the samples were heated to 2500 K at 21 GPa. As Fig. 3(a) shows, two new strong Raman peaks of annealed samples appear at room temperature, where the modes marked

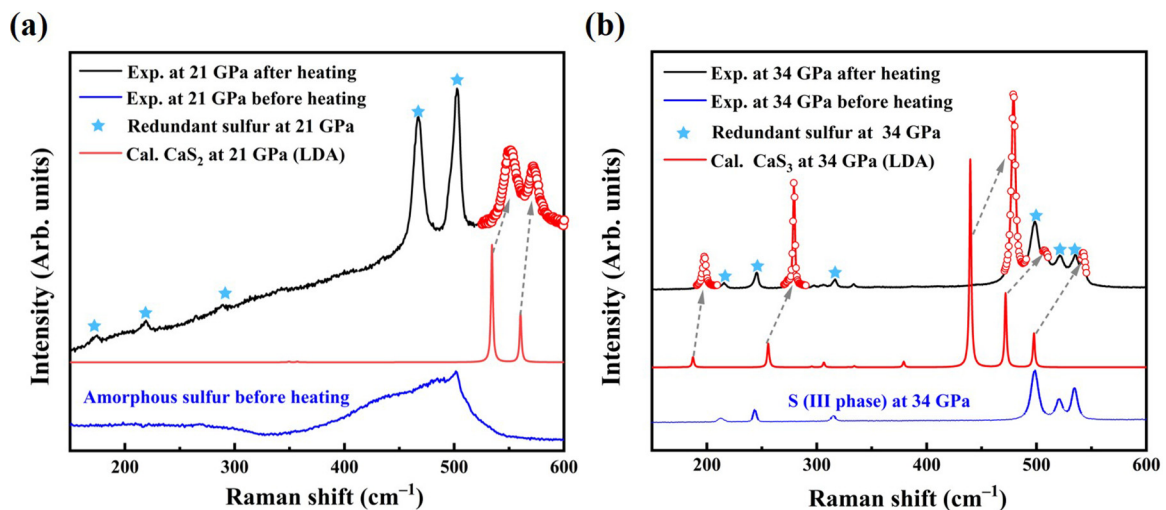


FIG. 3. Black/blue experimental and red calculated Raman spectra of (a)  $\text{CaS}_2$  at 21 GPa and (b)  $\text{CaS}_3$  at 34 GPa. At corresponding pressures, experimental Raman spectra of reactants before heating are marked by the blue lines at bottoms of the two panels. Raman signals of redundant sulfur are marked with blue stars.

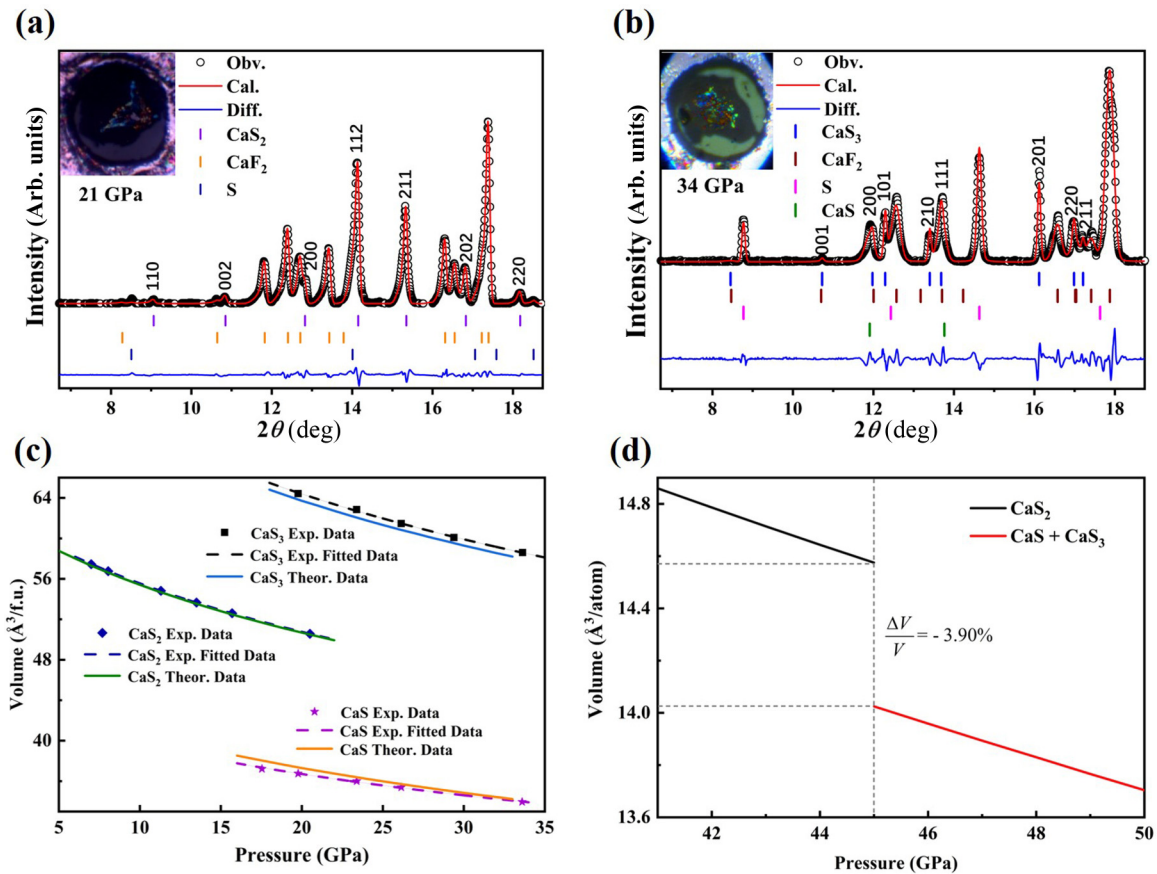


FIG. 4. The XRD patterns of (a)  $\text{CaS}_2$  and (b)  $\text{CaS}_3$  with the wavelength of  $0.6199 \text{ \AA}$ . The black open circles and red solid lines represent the Rietveld fits and observed data, respectively, and the blue solid lines are the residual intensity. Vertical ticks correspond to the Bragg positions of  $\text{CaS}_x$ ,  $\text{CaF}_2$ , and S; (c) volumes as a function of pressure for  $\text{CaS}_x$ . The symbols, dashed lines, and solid lines represent the experimental data, fits, and simulations of  $\text{CaS}_x$ , respectively. (d) The calculated volume shrinkage at about 45 GPa where the  $\text{CaS}_2$  compound is calculated to decompose into  $\text{CaS}$  and  $\text{CaS}_3$ .

by the star symbols are attributed to residual sulfur. Modes at  $551$  and  $572 \text{ cm}^{-1}$  belong to the stretching vibration of the  $\text{S}_2$  units, suggesting that the  $\text{CaS}_2$  compound has been synthesized. Encouraged by the successful synthesis of  $\text{CaS}_2$ , we attempted to obtain a  $\text{CaS}_3$  compound with higher S content and the samples were compressed to a higher pressure of 34 GPa and heated to about 2500 K, which is a more rigorous condition in contrast with that for previously synthesized  $\text{SrS}_3$  (5 GPa, 600 or 1200°C). The Raman spectrum of the heated sample at 34 GPa is collected and shown in Fig. 3(b), where the features of the laser heated pure sulfur sample are represented by the star symbols. Some strong modes are observed at about 197, 279, and  $478 \text{ cm}^{-1}$  indicating that the formation of a different phase. As the two elements (Sr, Ca) belong to the same main group, the stricter condition for  $\text{CaS}_3$  may be due to the relative weak activity of the calcium element, thus this also means that the reaction between calcium and sulfur should overcome a much higher energy barrier.

Usually, the uncertainty of precursors composition and temperature gradient effect, in complicated high-pressure-temperature experiments, prevents us from synthesizing a pure phase. Additionally, because of the preferred orientation in sample and other facts, the intensity of Raman may be changed for different experimental runs. All Raman spectra of

the samples were performed on same facility in our laboratory, thus full width at half maxima (FWHM) should be similar, which can be evidenced by the nearly equal FWHM of the redundant sulfur marked with blue stars in Fig. 3. The resolution of our Raman equipment is  $1.78 \text{ cm}^{-1}$ , which can distinguish the linewidths of these peaks. The wider linewidths of the presented Raman spectrum for  $\text{CaS}_2$  can be understood from two aspects: (i) Some unknown factors such as defect, etc., may be introduced in the crystallization process for the  $\text{CaS}_2$  compound which may weaken the signal of the Raman spectrum of  $\text{CaS}_2$  resulting in broadening of the peak linewidths. (ii) Based on the uncertainty principle, the wider linewidths may be from the shorter intrinsic phonon lifetime, which is perhaps associated with the anharmonic vibration of the  $\text{S}_2$  unit that is beyond the main topic of this study.

It is known that the LDA functional tends to overbind molecules and the usage of PBE functional for predicting vibrations may compensate for the error from neglecting quantum effects. Taking account of these complicated effects, we have compared the Raman spectra of  $\text{CaS}_2$  using different exchange correlation functions. The lattice parameters of unit cells employed for the GGA and LDA Raman simulations adopt the values from the structure relaxations using the corresponding exchange correlation functions. The Raman results

TABLE I. Bader charges in CaS, CaS<sub>2</sub>, and CaS<sub>3</sub> at 30 GPa.

	Ca ( <i>e</i> )	S/S1 ( <i>e</i> )	S2 ( <i>e</i> )	S/S <sub>2</sub> /S <sub>3</sub> unit ( <i>e</i> )
CaS (30 GPa)	1.301	-1.301		-1.301
CaS <sub>2</sub> (30 GPa)	1.310	-0.655		-1.310
CaS <sub>3</sub> (30 GPa)	1.364	-0.635	-0.094	-1.364

within GGA and LDA functional are similar, whereas the Raman results within the GGA functional show more obvious offsets compared to the experimental results, indicating that LDA functional could provide a better description for the vibrational properties of this Ca-S system. Our calculated Raman spectra of CaS<sub>2</sub> and CaS<sub>3</sub> at 21 and 34 GPa match up well with the results of experiments. More analysis demonstrates that two peaks of the CaS<sub>2</sub> Raman spectrum having different energies [Fig. 3(a)] belong to two different  $A_{1g}$  and  $B_{2g}$  vibrational modes. The strongest peak [Fig. 3(b)] at about 478 cm<sup>-1</sup> of CaS<sub>3</sub> can be assigned to the stretching vibration mode of the S<sub>3</sub> unit.

### C. Crystal structures and compressibilities

After the observation of anticipated Raman peaks of CaS<sub>2</sub> and CaS<sub>3</sub> from annealed samples, we performed the studies of their crystal structures and equation of states with the same samples.

In the direct two-dimensional (2D) XRD images and integrated patterns [Fig. 4(a)] two new distinct peaks at 14.2° and 16.8° and several weak ones appear that are not contained in the patterns of the other possible compounds (CaS, CaF<sub>2</sub>, and S). Contrasted with the calculated XRD patterns, we find that these two strong peaks located 14.2° and 16.8° can be refined well with the reflection of the (112) and (202) crystal planes of the predicted CaS<sub>2</sub> structure, respectively. As shown in Fig. 4(b), the further observed XRD patterns can be refined by the mixture of our proposed tetragonal CaS<sub>3</sub>, CaS, CaF<sub>2</sub>, and redundant elemental S. Especially, three selected strong peaks at 12.3°, 13.4°, and 16.1° match up well with the (101), (210), and (201) crystal planes of  $P-42_1m$ -CaS<sub>3</sub>.

The experiment lattices can be refined with the Rietveld method [Figs. 4(a) and 4(b)], where the relatively high fitted  $R$  values of 11.8% and 13.2% may be caused by the preferred orientation, the strongly anisotropic peak broadening effects, and especially, the multiphase in high-pressure-temperature synthesis. The experimental lattice parameters are in good agreement with those of our DFT simulations. Moreover, the evolution of the room-temperature XRD pattern as a function of pressure during decompression is given in the SM [38], where the features associated with CaS<sub>*x*</sub> are emphasized with blue vertical ticks. For CaS<sub>2</sub>, the features become weak gradually with the pressure decreasing. The peak around 21.6° refined with the reflection of (213) lattice plane could persist to 17.2 GPa and the one at about 15.2° refined with the reflection of (211) lattice plane disappears when the pressure is lower than 12.8 GPa. For CaS<sub>3</sub>, the signals become weaker but could persist to at least 19.8 GPa during decompression.

The calculated  $P$ - $V$  data of decompressions are fitted to a third order Birch-Murnaghan equation of state [42]:

$$P = \frac{3}{2}B_0 \left[ \left( \frac{V}{V_0} \right)^{-7/3} - \left( \frac{V}{V_0} \right)^{-5/3} \right] * \left\{ 1 + \frac{3}{4}(B'_0 - 4) * \left[ \left( \frac{V}{V_0} \right)^{-2/3} - 1 \right] \right\},$$

where  $B_0$  and  $B'_0$  represent the bulk modulus and its first derivative, and  $V_0$  is the equilibrium volume at zero pressure. The fitted experimental and theoretical compression behaviors of CaS, CaS<sub>2</sub>, and CaS<sub>3</sub> compounds are plotted in Fig. 4(c), which presents excellent consistency and further proves the credibility of calcium polysulfides. CaS<sub>2</sub> and CaS<sub>3</sub> show similar compressibility, whose  $B_0$  values are 56(8) and 51(7) GPa, respectively, while CaS has a slightly larger  $B_0$  with 59(8) GPa. In this system, the  $B_0$  values decrease with the sulfur content increasing, which indicates that the phase with higher sulfur content is prone to be compressed. At about 45 GPa, there is a slight volume shrinkage of  $\Delta V/V = -3.90\%$  between CaS<sub>2</sub> and 1/2 CaS<sub>3</sub> + 1/2 CaS [Fig. 4(d)]. It can be seen that the  $PV$  term of CaS and CaS<sub>3</sub> has the advantage with

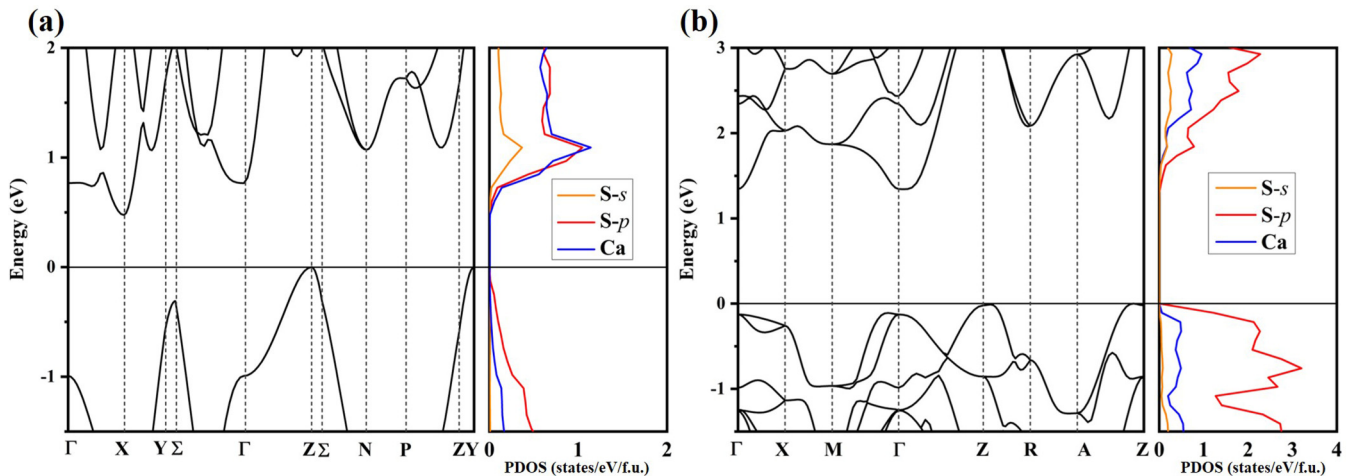


FIG. 5. Calculated band structures (left panel) and projected density of states (PDOS) (right panel) of (a) CaS<sub>2</sub> at 30 GPa and (b) CaS<sub>3</sub> at 30 GPa.

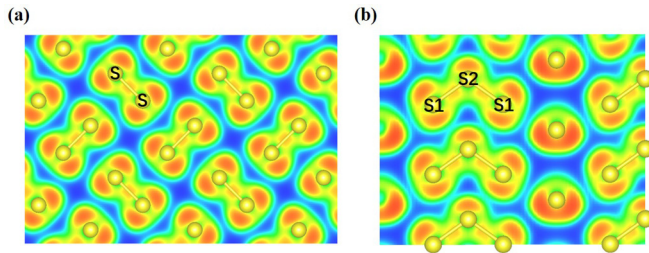


FIG. 6. Calculated electron localization functions (ELFs) of (a)  $\text{CaS}_2$  on (001) plane and (b)  $\text{CaS}_3$  on (110) plane at 30 GPa.

pressure increasing, thus  $\text{CaS}_2$  is energetically preferable at low pressure.

#### D. Electronic properties

After the successful syntheses, we further performed the simulations of the electronic properties of the calcium polysulfides. Commonly, sulfur takes the  $-2$  valence state resembling those in other chalcogenides. In this work, the increasing pressure stabilizes the polysulfide structure with the intriguing  $\text{S}_2$  and  $\text{S}_3$  subunits, which show corresponding  $\text{S}_2^{2-}$  and  $\text{S}_3^{2-}$  valences supported by our Bader charge analysis. For ionic compound, the value of electron transfer is lower than that of ideal valence state within the framework of Bader analysis. Thus,  $\text{CaS}$  is selected as a typical standard here, in which calcium is considered to lose all the  $s$ -orbit valence electrons and S show  $-2$  state. As Table I shows, each  $\text{S}_2$  subunit in  $\text{CaS}_2$  acquires  $\sim 1.31$  electrons from each calcium atom. In the  $\text{S}_3$  unit, each of the two edge sulfur atoms named S1 atom in [Fig. 6(b)] acquires approximately 0.64 electron, however, there is nearly no electron gained by the center atom [S2 atoms in Fig. 6(b)]. The sum of that electron transfer from the calcium atom to the  $\text{S}_3$  unit is totally equal to the value ( $1.30e$ ) of  $\text{CaS}$ . So, both  $\text{S}_2$  and  $\text{S}_3$  units show  $-2$  valence state.

The band structures and projected density of states (PDOS) are shown in Fig. 5.  $\text{CaS}_3$  and  $\text{CaS}_2$  are typical indirect band-gap semiconductors and the  $p$  orbit of sulfur atom is the main contribution near the Fermi energy level; that may be because the  $p$  orbits of the two sulfur atoms in the  $\text{S}_2$  units are fulfilled with the electrons deprived from calcium. Normally, the increasing pressure will gradually broaden the energy band and consequently cause the reduction of the band gap. Thus, the band gap of  $\text{CaS}_2$  decreases as expected. However, the band gap of  $\text{CaS}_3$  shows no significant variation as the pressure rises from 30 to 50 GPa (see the SM [38]). It is supposed that the reduction of the S-S-S bond angle will partially cancel the compression effect.

Figure 6 depicts the electron localization functions (ELFs) for each structure. According to the ELFs, bonds between the calcium and sulfur atoms that are strongly polar imply the ionic bonds. It is clearly seen that the large ELF values correspond to the obvious electronic locality between the S-S bonds which are all covalence bonds in the  $\text{CaS}_2$  and  $\text{CaS}_3$ . In  $\text{CaS}_3$ , the trimeric sulfur ( $\text{S}_3^{2-}$ ) units take a V shape for the existence of two lone electron pairs. To evaluate the bonding intensity of those structures, we also carried out the Laplacian of the electron density and the integration of the crystal orbital Hamiltonian population (ICOHP) analysis [43]. According to the atoms in molecules theory [44], the Laplacian of electron density  $\nabla^2\rho(r)$  of the bond critical points (BCPs) located between the bonding atoms could reveal the atomic interactions. The  $\nabla^2\rho(r)$  of these BCPs in the  $\text{S}_3$  units are  $-2.071$ , and the ones of the S-S bonds in the  $\text{CaS}_2$  are  $-2.965$ . They are all negative, indicating that the S-S bonds are covalent interactions. The integration of the crystal orbital Hamiltonian population (ICOHP) values up to the Fermi level scale are also analyzed. ICOHP values of S-S bonds are  $-5.407$  eV/bond of  $\text{CaS}_2$  and  $-5.523$  eV/bond of  $\text{CaS}_3$  respectively, indicating the S-S covalent bonds as well.

#### IV. CONCLUSIONS

In summary, we systematically explored the calcium polysulfides compounds up to 50 GPa in this joint theoretical and experimental study. Through high-pressure and high-temperature experiments, we have conclusively demonstrated the discovery of  $P-42_1m$ - $\text{CaS}_3$  and  $I4/mcm$ - $\text{CaS}_2$  structures with compelling  $\text{S}_3^{2-}$  and  $\text{S}_2^{2-}$  units, being identical with our predicted results. Under further compression, the disulfur unit is calculated to become unstable and evolves into the more favored trisulfur unit due to its lower energy. The present findings have elaborated the abundant calcium polysulfides and their detailed information under high pressure, providing a prominent exemplification for future investigations on polysulfides.

#### ACKNOWLEDGMENTS

This work was supported by the National Natural Science Foundation of China (Grants No. 12074139, No. 12034009, No. 11822404, No. 11774127, and No. 11974134), Interdisciplinary Integration and Innovation Project of Jilin University (Grant No. JLUXKJC2020311), and Strategic Priority Research Program of Chinese Academy of Sciences (Grant No. XDB33000000). We used the computing facilities at the High-Performance Computing Centre of Jilin University and Tianhe2-JK at the Beijing Computational Science Research Centre.

- [1] R. Pandey and S. Sivaraman, Spectroscopic properties of defects in alkaline-earth sulfides ravindra, *J. Phys. Chem. Solids* **52**, 211 (1991).  
 [2] S. Asano, N. Yamashita, and Y. Nakao, Luminescence of the  $\text{Pb}^{2+}$ -ion dimer center in  $\text{CaS}$  and  $\text{CaSe}$  phosphors, *Phys. Status Solidi* **89**, 663 (1978).

- [3] A. Shaikat, Y. Saeed, N. Ikram, and H. Akbarzadeh, First principles calculations of structural, electronic and optical properties of various phases of  $\text{CaS}$ , *Eur. Phys. J. B* **62**, 439 (2008).  
 [4] D. Varshney, N. Kaurav, R. Kinge, and R. K. Singh, High pressure structural ( $B1$ - $B2$ ) phase transition and elastic properties of

- II-VI semiconducting Sr chalcogens, *Comput. Mater. Sci.* **41**, 529 (2008).
- [5] L. Zhang, Y. Wang, J. Lv, and Y. Ma, Materials discovery at high pressures, *Nat. Rev. Mater.* **2**, 17005 (2017).
- [6] W. Zhang, A. R. Oganov, A. F. Goncharov, Q. Zhu, S. E. Boulfelfel, A. O. Lyakhov, E. Stavrou, M. Somayazulu, V. B. Prakapenka, and Z. Konopáková, Unexpected stable stoichiometries of sodium chlorides, *Science* **342**, 1502 (2013).
- [7] L. Zhu, H. Liu, C. J. Pickard, G. Zou, and Y. Ma, Reactions of xenon with iron and nickel are predicted in the earth's inner core, *Nat. Chem.* **6**, 644 (2014).
- [8] A. Dewaele, N. Worth, C. J. Pickard, R. J. Needs, S. Pascarelli, O. Mathon, M. Mezouar, and T. Irifune, Synthesis and stability of xenon oxides  $\text{Xe}_2\text{O}_5$  and  $\text{Xe}_3\text{O}_2$  under pressure, *Nat. Chem.* **8**, 784 (2016).
- [9] F. Peng, Y. Sun, C. J. Pickard, R. J. Needs, Q. Wu, and Y. Ma, Hydrogen Clathrate Structures in Rare Earth Hydrides at High Pressures: Possible Route to Room-Temperature Superconductivity, *Phys. Rev. Lett.* **119**, 107001 (2017).
- [10] S. Shao, W. Zhu, J. Lv, Y. Wang, Y. Chen, and Y. Ma, The exotically stoichiometric compounds in al-S system under high pressure, *Npj Comput. Mater.* **6**, 11 (2020).
- [11] H. Liu, I. I. Naumov, R. Hoffmann, N. W. Ashcroft, and R. J. Hemley, Potential high- $T_c$  superconducting lanthanum and yttrium hydrides at high pressure, *Proc. Natl. Acad. Sci. USA* **114**, 6990 (2017).
- [12] H. Wang, J. S. Tse, K. Tanaka, T. Iitaka, and Y. Ma, Superconductive sodalite-like clathrate calcium hydride at high pressures, *Proc. Natl. Acad. Sci. USA* **109**, 6463 (2012).
- [13] Y. Li, J. Hao, H. Liu, Y. Li, and Y. Ma, The metallization and superconductivity of dense hydrogen sulfide, *J. Chem. Phys.* **140**, 174712 (2014).
- [14] Q. Hu, D. Y. Kim, W. Yang, L. Yang, Y. Meng, L. Zhang, and H. K. Mao,  $\text{FeO}_2$  and  $\text{FeOOH}$  under deep lower-mantle conditions and earth's oxygen-hydrogen cycles, *Nature* **534**, 241 (2016).
- [15] S. Yamaoka, J. T. Lemley, J. M. Jenks, and H. Steinfiink, Structural chemistry of the polysulfides  $\text{Ba}_2\text{S}_3$  and  $\text{BaS}_3$ , *Inorg. Chem.* **14**, 129 (1975).
- [16] H. G. v. Schnering and N. K. Goh, Die strukturen der polysulfide  $\text{BaS}_3$ ,  $\text{SrS}_3$ ,  $\text{BaS}_2$ , und  $\text{SrS}_2$ , *Naturwissenschaften* **61**, 272 (1974).
- [17] I. Kawada, K. Kato, and S. Yamaoka, Strontium disulphide prepared at high pressure, *Acta Crystallogr., Sect. B* **32**, 3110 (1976).
- [18] H. Fukuoka, R. Suga, K. Komaguchi, S. Yamanaka, and M. Shiotani, New strontium polysulfides,  $\text{SrS}_3$ , and  $\text{Sr}_2(\text{OH})_2\text{S}_4 \cdot 10\text{H}_2\text{O}$ , obtained by the high-pressure treatment of a Sr-S mixture, *Inorg. Chem.* **43**, 5780 (2004).
- [19] N. Gong, C. Deng, L. Wu, B. Wan, Z. Wang, Z. Li, H. Gou, and F. Gao, Predicted semiconducting beryllium sulfides in 3D and 2D configurations: Insights from first-principles calculations, *J. Alloys Compd.* **781**, 371 (2019).
- [20] Y. Liu, C. Wang, S. Han, X. Chen, H. Sun, and X. Liu, Novel superconducting electrides in Ca-S system under high pressures, *Chin. Phys. Lett.* **38**, 036201 (2021).
- [21] Y. Wang, J. Lv, L. Zhu, and Y. Ma, Crystal structure prediction via particle-swarm optimization, *Phys. Rev. B* **82**, 094116 (2010).
- [22] Y. Wang, J. Lv, L. Zhu, and Y. Ma, CALYPSO: A method for crystal structure prediction, *Comput. Phys. Commun.* **183**, 2063 (2012).
- [23] B. Gao, P. Gao, S. Lu, J. Lv, Y. Wang, and Y. Ma, Interface structure prediction via calypso method, *Sci. Bull.* **64**, 301 (2019).
- [24] E. Stavrou, Y. Yao, A. F. Goncharov, S. S. Lobanov, J. M. Zaug, H. Liu, E. Greenberg, and V. B. Prakapenka, Synthesis of Xenon and Iron-Nickel Intermetallic Compounds at Earth's Core Thermodynamic Conditions, *Phys. Rev. Lett.* **120**, 096001 (2018).
- [25] M. Somayazulu, M. Ahart, A. K. Mishra, Z. M. Geballe, M. Baldini, Y. Meng, V. V. Struzhkin, and R. J. Hemley, Evidence for Superconductivity above 260 K in Lanthanum Superhydride at Megabar Pressures, *Phys. Rev. Lett.* **122**, 027001 (2019).
- [26] P. E. Blöchl, Projector augmented-wave method, *Phys. Rev. B* **50**, 17953 (1994).
- [27] J. P. Perdew, K. Burke, and M. Ernzerhof, Generalized Gradient Approximation Made Simple, *Phys. Rev. Lett.* **77**, 3865 (1996).
- [28] G. Kresse and J. Furthmüller, Efficient iterative schemes for ab initio total-energy calculations using a plane-wave basis set, *Phys. Rev. B* **54**, 11169 (1996).
- [29] J. P. Perdew and A. Zunger, Self-interaction correction to density-functional approximations for many-electron systems, *Phys. Rev. B* **23**, 5048 (1981).
- [30] K. Parlinski, Z. Q. Li, and Y. Kawazoe, First-Principles Determination of the Soft Mode in Cubic  $\text{ZrO}_2$ , *Phys. Rev. Lett.* **78**, 4063 (1997).
- [31] A. Togo, F. Oba, and I. Tanaka, First-principles calculations of the ferroelastic transition between rutile-type and  $\text{CaCl}_2$ -type  $\text{SiO}_2$  at high pressures, *Phys. Rev. B* **78**, 134106 (2008).
- [32] Y. Akahama and H. Kawamura, Pressure calibration of diamond anvil raman gauge to 410 GPa, *J. Phys. Conf. Ser.* **215**, 012195 (2010).
- [33] A. P. Hammersley, FIT2D: A multi-purpose data reduction, analysis and visualization program, *J. Appl. Crystallogr.* **49**, 646 (2016).
- [34] A. C. Larson and R. B. von Dreele, *GSAS: General Structure Analysis System* (Los Alamos National Laboratory, Los Alamos, NM, 1990).
- [35] B. H. Toby, EXPGUI, a graphical user interface for GSAS, *J. Appl. Crystallogr.* **34**, 210 (2001).
- [36] O. Degtyareva, E. Gregoryanz, M. Somayazulu, P. Dera, H. O. K. Mao, and R. J. Hemley, Novel chain structures in group VI elements, *Nat. Mater.* **4**, 152 (2005).
- [37] W. A. Crichton, G. B. M. Vaughan, and M. Mezouar, In situ structure solution of helical sulphur at 3 GPa and 400°C, *Z. Kristallogr.* **216**, 417 (2001).
- [38] See Supplemental Material at <http://link.aps.org/supplemental/10.1103/PhysRevB.104.054117> for the phonon dispersion curves, estimated pressure-temperature phase diagram, Raman spectra, x-ray diffraction patterns under decompression, calculated bandgaps, and crystal information of  $\text{CaS}_x$  under pressures.
- [39] J. R. Nelson, R. J. Needs, and C. J. Pickard, Calcium peroxide from ambient to high pressures, *Phys. Chem. Chem. Phys.* **17**, 6889 (2015).
- [40] J. Li, H. Y. Guo, D. M. Proserpio, and A. Sironi, Exploring tellurides: Synthesis and characterization of new binary, ternary, and quaternary compounds, *J. Solid State Chem.* **117**, 247 (1995).

- [41] Y. Wang, M. Xu, L. Yang, B. Yan, Q. Qin, X. Shao, Y. Zhang, D. Huang, X. Lin, J. Lv, D. Zhang, H. Gou, H. kwang Mao, C. Chen, and Y. Ma, Pressure-stabilized divalent ozonide  $\text{CaO}_3$  and its impact on earth's oxygen cycles, *Nat. Commun.* **11**, 4702 (2020).
- [42] F. Birch, Section of geology and mineralogy: Elasticity and constitution of the earth's interior, *J. Geophys. Res.* **57**, 227 (1952).
- [43] R. Dronskowski and P. E. Blöchl, Crystal orbital hamilton populations (COHP): energy-resolved visualization of chemical bonding in solids based on density-functional calculations, *J. Phys. Chem.* **97**, 8617 (1993).
- [44] R. Bochicchio, R. Ponc, A. Torre, and L. Lain, Multicenter bonding within the AIM theory, *Theor. Chem. Acc.* **105**, 292 (2001).